The Appearance and Disappearance of Ship Tracks on Large Spatial Scales

J. A. COAKLEY JR.,[*] P. A. DURKEE,[+] K. NIELSEN,[+] J. P. TAYLOR,[#] S. PLATNICK,[@]
B. A. ALBRECHT,[&] D. BABB,[**] F-L. CHANG,[*] W. R. TAHNK,[*]
C. S. BRETHERTON,[++] AND P. V. HOBBS[++]

[*] *College of Oceanic and Atmospheric Sciences, Oregon State University, Corvallis, Oregon*
[+] *Department of Meteorology, Naval Postgraduate School, Monterey, California*
[#] *Meteorological Research Flight, The Met. Office, Farnborough, Hampshire, United Kingdom*
[@] *NASA Goddard Space Flight Center, Greenbelt, Maryland*
[&] *RSMAS/MPO, University of Miami, Coral Gables, Florida*
[**] *Department of Meteorology, The Pennsylvania State University, University Park, Pennsylvania*
[++] *Atmospheric Science Department, University of Washington, Seattle, Washington*

ABSTRACT

The 1-km advanced very high resolution radiometer observations from the morning, *NOAA-12,* and afternoon, *NOAA-11,* satellite passes over the coast of California during June 1994 are used to determine the altitudes, visible optical depths, and cloud droplet effective radii for low-level clouds. Comparisons are made between the properties of clouds within 50 km of ship tracks and those farther than 200 km from the tracks in order to deduce the conditions that are conducive to the appearance of ship tracks in satellite images. The results indicate that the low-level clouds must be sufficiently close to the surface for ship tracks to form. Ship tracks rarely appear in low-level clouds having altitudes greater than 1 km. The distributions of visible optical depths and cloud droplet effective radii for ambient clouds in which ship tracks are embedded are the same as those for clouds without ship tracks. Cloud droplet sizes and liquid water paths for low-level clouds do not constrain the appearance of ship tracks in the imagery. The sensitivity of ship tracks to cloud altitude appears to explain why the majority of ship tracks observed from satellites off the coast of California are found south of 35°N. A small rise in the height of low-level clouds appears to explain why numerous ship tracks appeared on one day in a particular region but disappeared on the next, even though the altitudes of the low-level clouds were generally less than 1 km and the cloud cover was the same for both days. In addition, ship tracks are frequent when low-level clouds at altitudes below 1 km are extensive and completely cover large areas. The frequency of imagery pixels overcast by clouds with altitudes below 1 km is greater in the morning than in the afternoon and explains why more ship tracks are observed in the morning than in the afternoon. If the occurrence of ship tracks in satellite imagery data depends on the coupling of the clouds to the underlying boundary layer, then cloud-top altitude and the area of complete cloud cover by low-level clouds may be useful indices for this coupling.

1. Introduction

Perusal of advanced very high resolution radiometer (AVHRR) satellite imagery gives the impression that ship tracks are confined to low-level, stratus, and stratocumulus. Off the coast of California such clouds abound in late spring and early summer. Nevertheless, as is shown in Fig. 1 for the June 1994 Monterey Area Ship Track (MAST) experiment, ship tracks appeared to form in certain locations and not in others. Furthermore, the preferred locations do not seem to reflect the density of weather reports from ships, shown in Fig. 2, which is taken to be indicative of ship traffic. In ad-

dition, on days when ship tracks occur, they seem to be plentiful. On days when ship tracks fail to materialize, even a hint of a ship track is difficult to discern despite the abundance of low-level clouds. For example, during MAST the afternoon *NOAA-11* AVHRR observations on 14 June showed numerous ship tracks, as shown in Fig. 3, and the observations on 15 June showed few ship tracks, even though the clouds for the two days appeared to be similar. The preferences for certain locations and the on–off behavior of ship tracks over relatively large spatial scales suggest that the susceptibility of clouds to ship track formation is not governed solely by local-scale cloud processes but subject to large-scale forcing as well.

Radiative transfer theory coupled with rudimentary models for the condensational growth of cloud droplets suggests that the appearance of ship tracks is affected by the preexisting state of the clouds. Platnick and

---

Corresponding author address: Dr. James A. Coakley Jr., College of Oceanic and Atmospheric Sciences, Oceanography Admin. 104, Oregon State University, Corvallis, OR 97331-5503.
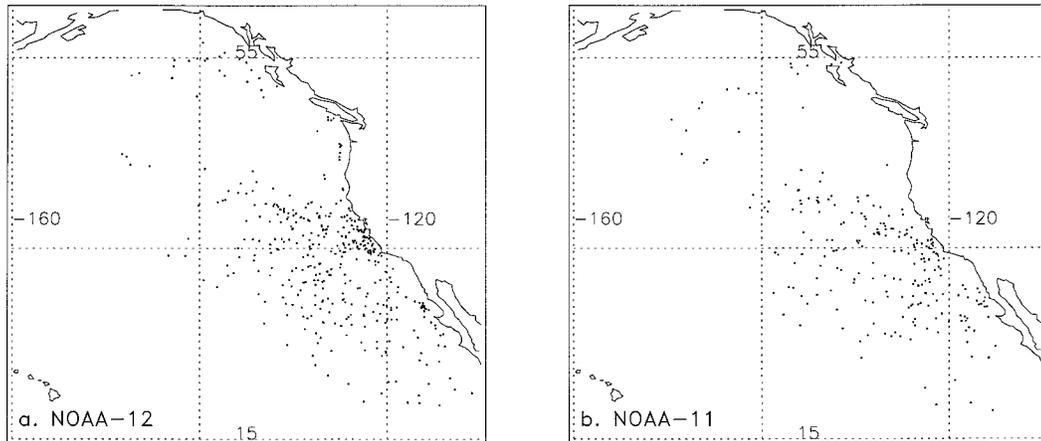E-mail: coakley@oce.orst.edu

FIG. 1. Locations of ship track heads, the end of the track thought to be nearest the ship, for the morning *NOAA-12* (a) and afternoon *NOAA-11* (b) passes for Jun 1994.

Twomey (1994) labeled this preconditioning as "cloud susceptibility." Here it will be referred to as "radiative susceptibility" in order to distinguish it from what would appear to be a "thermodynamic susceptibility." A possible mechanism for the thermodynamic susceptibility is the degree of coupling between the low-level clouds and the marine boundary layer (Nicholls 1984). If this coupling is weak or intermittent, then the particles in the ship plumes will be less likely to reach the clouds and thereby affect the radiative properties of the clouds.

The two forms of susceptibility are distinguishable. Radiative susceptibility is governed by the number of cloud droplets per unit volume, the vertical thickness of the cloud, and the size of the droplets. Clouds that are geometrically thin and have few, but large, droplets are more susceptible to increases in cloud condensation nuclei than are clouds that are geometrically thick and have many, but small, droplets (Platnick et al. 2000). Cloud droplet number concentration, geometrical thick-

ness, and droplet radii are related to the visible optical depth of a cloud and to the cloud reflectivity in the near-infrared (Arking and Childs 1985; Nakajima et al. 1991; Han et al. 1994; Platnick and Valero 1995). The degree of coupling between a low-level cloud layer and the marine boundary layer, on the other hand, might be manifested by regional or day-to-day shifts in cloud height and cloud cover. Climatological evidence (Albrecht et al. 1995) and modeling studies (Krueger et al. 1995a,b; Wyant et al. 1997) indicate that broken clouds with higher altitudes are less likely to be coupled to the boundary layer than are overcast clouds with lower altitudes.

Here AVHRR radiances at 0.63, 3.7, and 11 μm are analyzed for the fractional cloud cover, optical depths at 0.63 μm, cloud droplet effective radii, and cloud heights for low-level clouds. These results are combined with the positions of ship track heads found in satellite imagery in order to compare the properties of the clouds
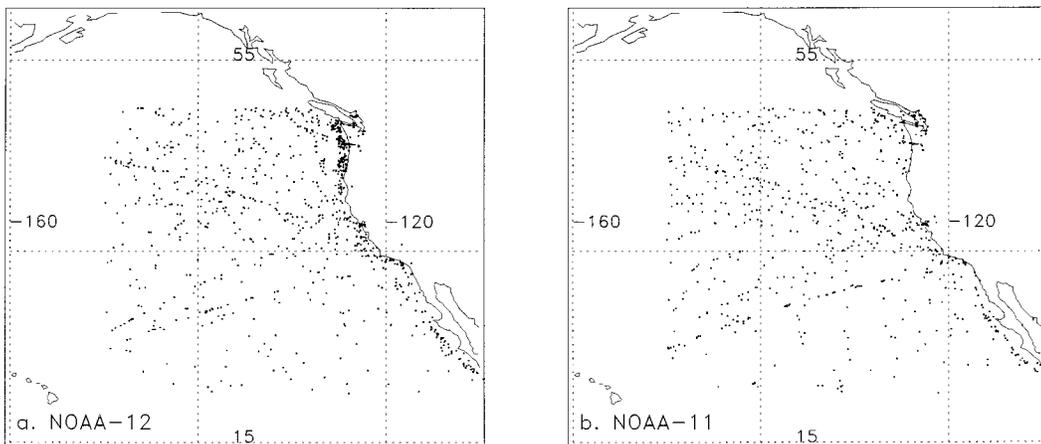

FIG. 2. Locations of weather reports from ships within ± 2 h of the morning *NOAA-12* (a) and afternoon *NOAA-11* (b) passes. The reports are for Jun 1994.

in which ship tracks were observed with those of the clouds in which ship tracks were not found. These comparisons lead to the finding that the appearance of ship tracks in satellite imagery is governed more by the apparent coupling of the clouds to the marine boundary layer, as manifested in terms of cloud height and the frequency of overcast imagery pixels, rather than by the radiative properties of the preexisting clouds. The findings are used to explain the preference for track formation south of 35°N, as shown in Fig. 1; the higher frequency of track sightings in the morning *NOAA-12* observations; and the appearance of tracks on 14 June and their disappearance on 15 June.

2. Data analysis

The 1-km AVHRR observations for the afternoon passes of the *NOAA-11* satellite and the morning passes of the *NOAA-12* satellite over the California coast were analyzed using the spatial coherence method (Coakley and Baldwin 1984). The method identifies pixels that are 1) overcast by layered clouds, 2) cloud-free, and 3) partly cloud covered or covered by clouds that exhibit considerable vertical variations within the 1-km field of view. The satellite coverage for MAST allowed analysis of the region from 30° to 45°N and from 140°W to the California coast. The coverage for *NOAA-11* reached south to 25°N, but for *NOAA-12,* the coverage was intermittent south of 30°N. The results of the spatial coherence analysis were collected for 60-km-scale (64 scan spot $\times$ 64 scan line) regions. For each region, the averages and standard deviations of the radiances for those pixels found to be either cloud-free or completely covered by layered clouds were saved. The numbers of cloud-free and overcast pixels within each region were also saved.

The average radiances of pixels identified by the spatial coherence method as being cloud-free for the 60-km-scale regions were first used to obtain the radiances associated with the cloud-free ocean background. Daily values of these cloud-free radiances were composited to generate a monthly mean model that gave the radiances as functions of the latitude and the sun–target–satellite viewing geometry. These radiances were used to estimate the cloud-free radiances when there were no cloud-free pixels in the vicinity ($\sim$250 km) of the region being analyzed on the day of the pass. When there were cloud-free pixels within the vicinity, spatial interpolation was used to estimate the cloud-free radiances within the region being analyzed. Rms differences between observed cloud-free radiances and those derived either through spatial interpolation or from the climatology were generally smaller than 1.3 K for the SST and 0.01 for the 0.63-μm reflectivity.

Procedures similar to those described by Han et al. (1994) were used to derive visible optical depths, emission temperatures, and cloud droplet radii for low-level clouds from the AVHRR radiances observed at 0.63,

3.7 and 11 μm. The retrievals were performed using the means of the radiances for the pixels identified by the spatial coherence analysis as being overcast by low-level cloud within the 60-km-scale regions. The retrievals were performed only for oceanic regions. Continental regions and oceanic regions within 60 km of the coast were not analyzed. An adding–doubling radiative transfer routine was used to generate tables of the radiative properties at 0.63, 3.7, and 11 μm for plane-parallel, homogeneous clouds having various sets of 0.63-μm optical depths and effective droplet radii. The routine had 16 streams in both the upward and downward directions. The δ–M method described by Wiscombe (1977) was used to treat the forward scattering peak of the phase function. Mie scattering was used to treat the scattering by water droplets. The correlated-k models for atmospheric absorption developed for the AVHRR channels by Kratz (1995) were used to correct for atmospheric effects. Temperatures and humidities for the retrievals were taken from the radiosondes launched from the R/V *Glorita* (Syrett 1994) at the time nearest the satellite overpass. At altitudes not reached by the sounding, temperatures and humidities were taken from a midlatitude summertime climatology. Cloud-free radiances at 11 μm derived from the spatial coherence analysis of the satellite observations were used to derive a consistent sea surface temperature for the retrievals. Corrections were made for the Sun–Earth distance in calculating the reflected radiances at 0.63 and 3.7 μm and for the calibrations of the 0.63-μm channels of the *NOAA-11* (Rao and Chen 1995) and the *NOAA-12* (Loeb 1997) AVHRRs.

Results from the retrieval scheme were compared with those derived from the routine developed by Platnick and Valero (1995) and used by Platnick et al. (2000). The ensemble of cases in the comparison had retrieved cloud droplet radii ranging from 4 to 30 μm and visible optical depths ranging from 1 to 20. The rms difference for the effective radii retrieved with the two schemes was less than 1 μm, and the current scheme retrieved a 0.63-μm optical depth that was typically 10% larger than that obtained with the Platnick et al. scheme and the rms differences were within 1 unit in optical depth about the mean difference. These comparisons indicate that the results obtained using the current scheme would differ little from those obtained by others (Han et al. 1994; Platnick and Valero 1995; Nakajima and Nakajima 1995). Because the differences tended to grow for cases at relatively large satellite zenith angles ($>$45°), the satellite zenith angles for the results reported later were restricted to be less than 30°.

NOAA-11 and *NOAA-12* satellite imagery were manually analyzed to identify ship tracks and locate the heads of the tracks. The ship track head is at the end of the track thought to be closest to the ship at the time of the satellite overpass. The locations of the heads were used to identify the 60-km regions that contained clouds that were evidently susceptible to track formation.

NOAA-11
JUNE 14, 1994 0044Z
0.89-μm

3.7-μm

11-μm

NOAA-11
JUNE 15, 1994 0032Z
0.89-μm

3.7-μm
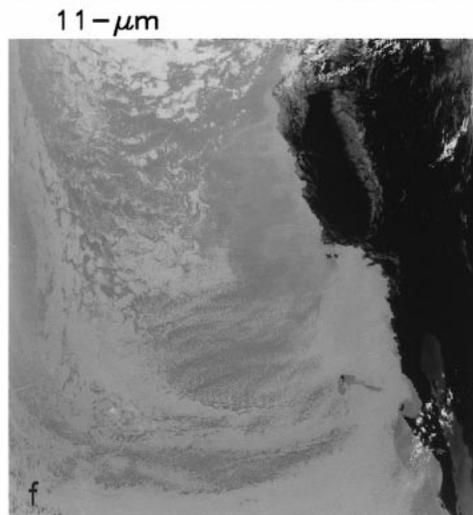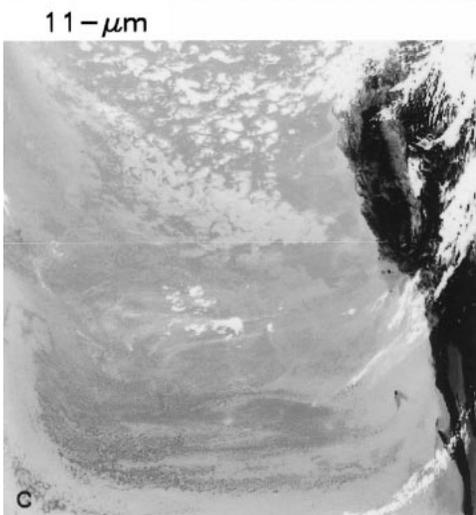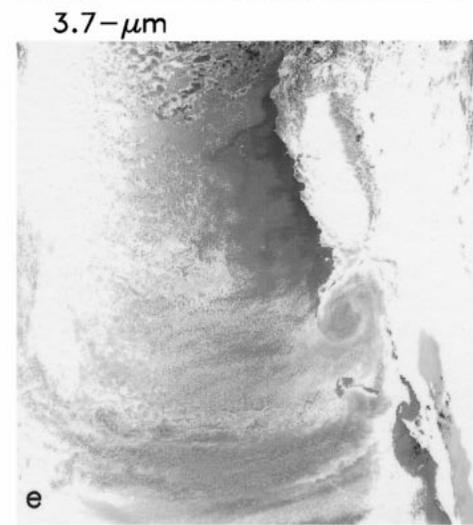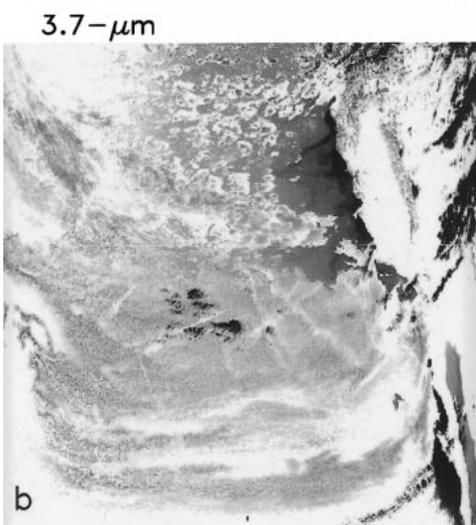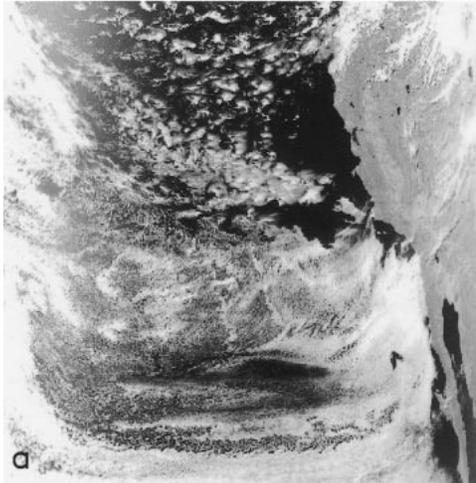
11-μm

Cloud-free and overcast 11-μm radiances were converted to brightness temperatures using the instrument response functions for the *NOAA-11* and *NOAA-12* AVHRRs, and the instruments were calibrated following the linear method described by Lauritsen et al. (1979). Brightness temperatures for cloud-free pixels and pixels overcast by low-level clouds were used to obtain the difference between the sea surface temperature (SST) and cloud-top temperatures. Assuming a constant lapse rate, this difference should provide a reliable estimate of cloud-top altitude, at least for low-level clouds (Betts et al. 1992).

To test such estimates of cloud altitude, differences between cloud-top and surface air temperatures obtained from the soundings made from the R/V *Glorita* and by the U.K. Meteorological Office C-130 aircraft were compared with those derived from the *NOAA-11* and *NOAA-12* satellite observations. The soundings selected for comparison all had inversion strengths, ΔT, that were at least 3 K. The temperature at the base of the inversion was taken to be the cloud-top temperature. Also, the selected soundings all had surface air temperatures, or in the case of the C-130 the lowest-level air temperatures, and inversion base temperatures that differed by more than 2 K. Ninety-four soundings were launched from the R/V *Glorita*. Of the 94, 74 had suitable inversions. Of these, 24 were within ± 4 h of the afternoon pass of the *NOAA-11* satellite and 24 were within ± 4 h of the morning *NOAA-12* pass. Of these 48 soundings, 32 were associated with satellite passes in which pixels were found to be overcast by low-level clouds that were within 150 km of the sounding. For the remaining 16 cases, no overcast fields of view were found within 150 km of the radiosonde observations. The satellite estimates for cloud-top temperatures in these cases were derived through interpolation of the values obtained from overcast fields of view in nearby ($<$60 km) regions when overcast fields of view were found in these surrounding regions. Such estimates of cloud-top temperatures, however, were suspected of being less reliable than those obtained from the overcast fields of view within 150 km of the radiosonde observations and were therefore not included in the comparisons. For the C-130, 15 soundings were taken over the open ocean more than 100 km from the coast. Of these, 12 had suitable inversions and 8 were within ± 4 h of the *NOAA-11* and *NOAA-12* passes. For 7 of the soundings, the associated passes had pixels overcast by low-level clouds that were within 150 km of the sounding. The average 11-μm brightness temperatures for the overcast pixels within 150 km of the sounding were taken to be the cloud-top temperature. The differences between these temperatures and the 11-μm brightness temperatures expected for the cloud-free ocean were taken to be the differences between the cloud-top and surface temperatures.

In addition to the soundings, comparisons were also made between the satellite-derived SST and measurements made with a radiative probe from the C-130 and with a skin temperature probe from the R/V *Glorita.* For the C-130, the SST was obtained by converting 8–14-μm radiances measured with a Barnes PRT-4 to brightness temperatures. The PRT-4 was calibrated in flight with an onboard blackbody. The temperature of the blackbody was varied to cover a range that exceeded the brightness temperatures that were being observed. For the R/V *Glorita,* the measurements were obtained using a precision thermistor that was placed at the end of a tygon tube and dragged behind the ship (Fairall et al. 1997).

The use of brightness temperatures for the SST and cloud-top temperatures, and the neglect of the corrections for atmospheric absorption and emission and for the nonlinearities in the calibration of the 11- and 12-μm radiances obtained with the AVHRRs (Weinreb et al. 1990), requires justification. Corrections for absorption and emission, primarily by water vapor in the atmosphere, cause the observed 11-μm cloud-free temperature to be 1–2 K below the SST according to both the routine procedures for extracting SSTs from AVHRR data (McMillan and Crosby 1984; Prata 1993) and also the surface temperatures obtained by comparing observed and calculated radiances using the retrieval scheme described above. Nevertheless, direct comparison of the brightness temperatures with the in situ observations, as discussed in the next section, showed good agreement. Furthermore, since corrections for the SST are generally $\sim$1–2 K and those for the cloud-top temperature are generally $\sim$1 K in the same sense, the separate errors of the SST and cloud-top temperature cancel when differences are taken to determine cloud-top altitude.

3. Retrieved and in situ measurements of SST, cloud-top temperature, and surface–cloud-top temperature difference

Figure 4 shows the satellite retrievals and the sounding estimates of the surface temperature, the cloud-top temperature, and differences between the surface and cloud-top temperatures. The crosses in Fig. 4 are for the C-130 soundings; the boxes are for the R/V *Glorita* soundings. As was noted in the previous section, all cases are for single-layered, low-level clouds. The figure

←

FIG. 3. Images constructed from 0.89-, 3.7-, and 11-μm radiances for the afternoon passes of the *NOAA-11* on 14 and 15 Jun 1994. On 14 Jun, numerous ship tracks were found in the low-level clouds off the coast of CA. On 15 Jun, few tracks were found yet the cloud systems appeared to be similar.
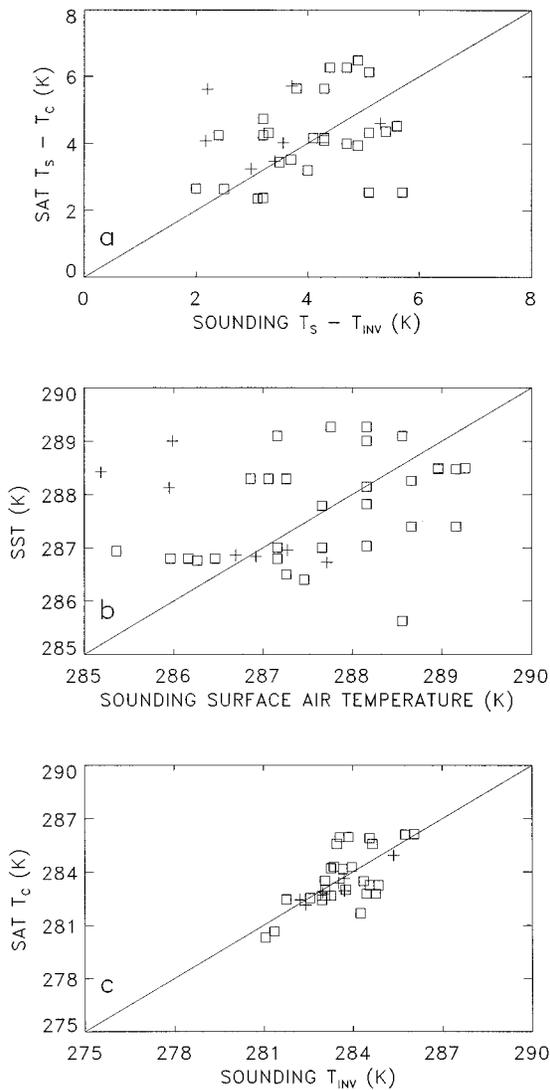
FIG. 4. Differences between surface temperatures and cloud-top temperatures deduced from the satellite radiances and the soundings for cases in which overcast pixels were found in a single-layered cloud system within 150 km and ±4 h of the sounding (a), SSTs derived from the 11-μm radiances and surface air temperatures derived from the soundings (b), and cloud-top temperatures derived from 11-μm radiances and from the base temperatures of the inversions (c). Boxes indicate comparisons between the satellite and the R/V *Glorita* soundings; crosses indicate comparisons between the satellite and the C-130 aircraft soundings. The observations were collected as part of MAST in Jun 1994.
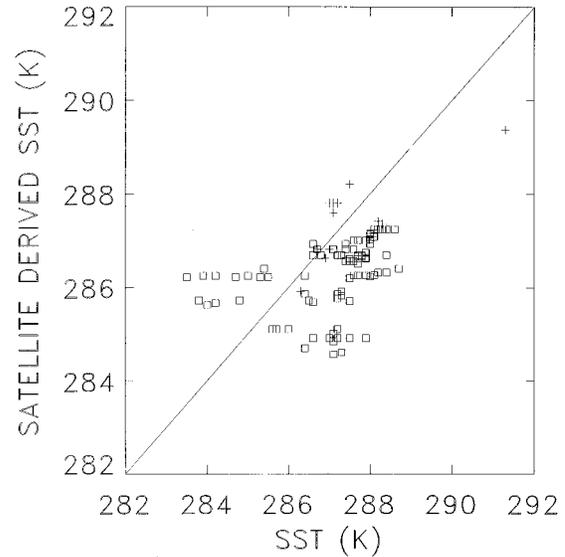

FIG. 5. SSTs derived from 11-μm radiances and in situ SST probes for cases when the satellite observed cloud-free pixels within 150 km and ±8 h of the probe measurements. Boxes indicate comparisons between the satellite and the R/V *Glorita* observations; crosses indicate comparisons between the satellite and the C-130 aircraft observations. The observations were collected as part of MAST in Jun 1994.

shows that even for the small range of variability in the in situ observations, the satellite estimates of the difference between the surface and cloud-top temperatures followed the value inferred from the in situ measurements. The satellite estimates of the differences in surface and cloud-top temperatures were generally within ±2 K of the differences derived from the soundings. For a lapse rate of 7 K km⁻¹ (Betts et al. 1992), ±2 K corresponds to a ±300-m range in altitude.

The departures of the satellite-derived surface–cloud-top temperature differences from the differences inferred from in situ observations can be explained by the departures of the satellite SST and cloud-top emission temperature from the in situ observations of the SST and the temperature at the base of the low-level inversion. For the most part, there were no cloud-free pixels within 150 km of the soundings for the results shown in Fig. 4. The SSTs shown in Fig. 4 were derived primarily through interpolation from observations of cloud-free fields of view at relatively large distances (>150 km) from the sounding and from the model for the cloud-free radiances discussed in section 2. As was also noted in section 2 and as shown in Fig. 4, the SSTs inferred from the analysis of the satellite observations were typically within ±1 K of the surface air temperature. Figure 5 shows SSTs derived for cloud-free pixels within 150 km of measurements taken from the C-130 and R/V *Glorita* SST probes within 8 h of the satellite pass. Again, the SSTs derived from the cloud-free pixels were within ±1 K of the in situ measurements. The differences shown are similar to the differences between the SSTs measured by the R/V *Glorita* and by the C-130 when they were within 150 km and 8 h of each other. Figure 4 also shows the cloud-top temperatures derived from overcast pixels within 150 km of the in situ soundings for passes that occurred within ±4 h of the soundings. The departures of the cloud-top temperatures from those at the base of the inversion were ±2 K. Despite the small range in the observations, the satellite esti-
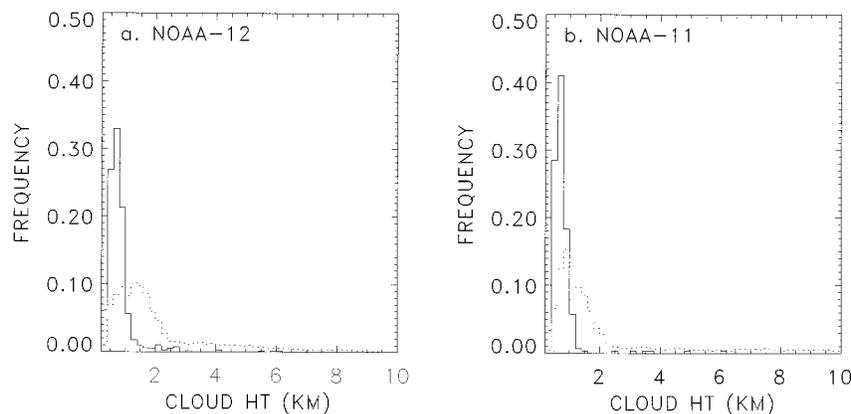
FIG. 6. Altitudes of the uppermost clouds found in 60-km regions within 50 km of a ship track head (solid line) and in regions more than 200 km from a ship track head (dashed line). The observations are for ocean regions off the west coast of the United States for Jun 1994.

mates track those inferred from the in situ measurements.

4. Retrieved properties of clouds with and without ship tracks

Figure 6 shows the distribution of altitudes for the uppermost clouds found within the 60-km regions analyzed. The altitudes were derived by taking the difference between the 10th percentile of the 11-μm brightness temperature and the cloud-free 11-μm brightness temperature observed for each 60-km-scale region and assuming a constant lapse rate of 7 K km^{-1}. The dashed line is for 60-km regions that are more than 200 km from a ship track head, and the solid line is for 60-km regions within 50 km of a ship track head. The frequencies are normalized so that they sum to unity. Because ship tracks are relatively rare, the results for the regions without ship tracks can be taken to be the distribution of cloud altitudes in the region off the California coast for June 1994. Because of the well-known diurnal variability of marine stratocumulus, two figures are shown: one for the morning *NOAA-12* passes and one for the afternoon *NOAA-11* passes.

The distribution of altitudes for the uppermost clouds indicates that the vast majority of clouds over the ocean in June 1994 were low-level. The regions with ship tracks and the regions without show the unmistakable peak in frequency caused by ubiquitous low-level marine stratocumulus. Based on the distribution of altitudes, 2.6 km was taken to be a suitable value for the maximum altitude associated with low-level clouds. The results for the regions without ship tracks show the presence of some upper-level systems, altitudes >2.6 km, but the appearance of upper-level clouds was relatively rare. On rare occasions, upper-level clouds were also found in the 60-km regions that contained a ship track head. When upper-level clouds were present together with a ship track, the ship track appeared in a low-level

cloud layer. The simultaneous occurrences of ship tracks and upper-level clouds are indicated in the figure as those occasions for which the altitude of the ship track case is well above the altitudes associated with low-level clouds. Based on the results shown in the figure, upper-level clouds masking low-level clouds was not a major cause for the disappearance of the ship tracks.

Figure 7 shows the fractional cloud cover, cloud altitudes, 0.63-μm optical depths, and cloud droplet effective radii for 60-km regions within 50 km of a ship track (solid line) and those farther than 200 km from a track (dashed line). As discussed in section 2, the values presented here are for the averages of the overcast pixels within 60-km regions that contained a single-layered, low-level cloud. The frequencies are normalized so that the sum of the frequencies is unity. Figures 7a–d show results for the morning *NOAA-12* observations and Figs. 7e–h show results for the afternoon *NOAA-11* observations. As indicated in section 2, all of the observations shown in Fig. 7 are for ocean scenes.

The most striking feature to come from the comparisons of clouds with and without ship tracks is that ship track heads occurred only when the low-level clouds within the 60-km regions were especially low. The restriction of the ship tracks to the lowest of the low-level clouds is consistent with the presence of ship tracks near the R/V *Glorita* at the times of the soundings (Durkee et al. 2000). The lack of tracks for higher clouds may be due to no, or intermittent, coupling between the low-level clouds and the boundary layer (Nicholls 1984). As Klein et al. (1995) noted, a common occurrence in the eastern North Pacific is for a well-mixed boundary layer to extend from the surface to approximately 500 m. At the top of the boundary layer cumulus clouds have their bases in localized regions subject to convective updrafts. The cumulus clouds then extend to a layer that contains stratus and stratocumulus at an altitude that may be as high as 1600 m. The area covered by the stratus and stratocumulus is more extensive than the
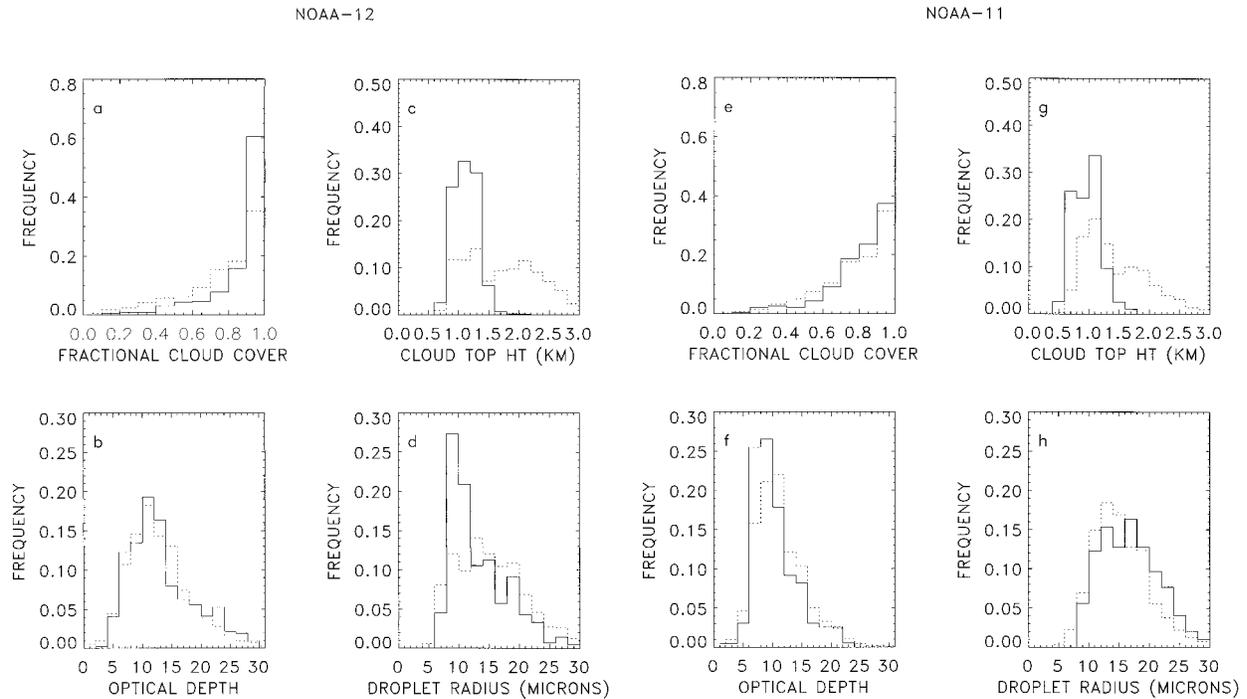
NOAA−12　　　　　　　　　　　　　　　　　　　NOAA−11

FIG. 7. Frequencies of fractional cloud cover, cloud-top altitude, 0.63-μm optical depth, and cloud droplet effective radius for 60-km regions within 50 km of a ship track head (solid line) and for regions that were more than 200 km from a ship track head (dashed line) for Jun 1994. The cloud altitudes, optical depths, and droplet radii were derived from the average radiances for the pixels found to be overcast within the 60-km regions. The observations are for ocean regions only. Morning *NOAA-12* observations (a)–(d); afternoon *NOAA-11* observations (e)–(h).

area covered by the underlying cumulus. The cumulus clouds connect the stratus and stratocumulus layer to the underlying boundary layer. It would appear from the results in Fig. 7 that if the ship tracks appear when the cloud layer is well coupled to the boundary layer, and the ship tracks disappear when the cloud layer becomes decoupled or poorly coupled, then the transition from coupled to decoupled occurs when the clouds have altitudes of about 1 km. This transition is the same for both the morning and the afternoon observations. This result is consistent with findings from soundings at four marine sites frequented by low-level clouds (Albrecht et al. 1995) and from numerical modeling of the marine boundary layer (Krueger et al. 1995a,b; Wyant et al. 1997) that suggest that the transition from well-coupled to decoupled or poorly coupled occurs for low-level clouds with altitudes between 1 and 1.5 km.

It should be recognized that the absence of ship tracks in satellite imagery does not mean that the clouds are unaffected by particles from the ships. When the overlying stratus or strato-cumulus cloud layer is only weakly coupled to the boundary layer, particles in the boundary layer might still be entering these clouds. The absence of ship tracks may simply indicate that where the overlying cloud layer is coupled by cumulus to the boundary layer, the concentration of the particles from the ship may be low, due to dispersion in the boundary layer or to the proximity of the locations of boundary

layer and cloud layer coupling relative to the ship plume. Also, if the concentration of particles is not low, the points of coupling may be sufficiently rare that a recognizable ship track fails to appear in the upper-level clouds. It should be recognized that if the low-level clouds above 1 km were coupled to the boundary layer, then the additional dispersion arising from the added depth of the mixed layer appears to be insufficient to explain the disappearance of the ship tracks. The evidence that the additional dispersion would be unlikely to cause the disappearance is that ship tracks often extend tens, and even hundreds, of kilometers from the head, and at these distances, they suffer considerable horizontal dispersion and broadening without disappearing. Finally, it should also be noted that not all ships will produce tracks. Even when appropriate cloud and environmental conditions exist, the formation of a ship track depends on the nature of the fuel, the ship's engine type, power output, etc. (Hobbs et al. 2000).

In addition to the dependence of ship track observations on cloud altitude, the results in Fig. 7 indicate that the 60-km regions near the ship tracks are more often overcast than those farther away from the tracks. It may simply be easier to detect the tracks in the imagery when the cloud cover is extensive, but, as will be discussed below, the occurrence of ship tracks appears to be linked to the frequency with which the 1-km AVHRR pixels are overcast by clouds that are suffi-

ciently low for tracks to occur. Again, the results in Fig. 7 are for 60-km regions that contain only a single-layered, low-level cloud and for which some of the 1-km pixels within the region are overcast. Evidently, when such conditions occur, the cloud cover within the 60-km region is relatively high.

Figure 7 shows that the optical depths and cloud droplet radii were nearly the same for clouds with and without ship tracks for both the morning, *NOAA-12,* and the afternoon, *NOAA-11,* observations. For the morning *NOAA-12* observations, clouds without ship tracks had, on average, slightly larger cloud droplet effective radii than clouds with ship tracks. As discussed below, in some of the morning observations, the larger cloud droplet effective radii were found in clouds with higher altitudes. Because of the higher altitudes, these clouds were less susceptible to the occurrence of ship tracks. The lack of differences for both optical depths and cloud droplet radii between clouds with and without ship tracks indicates that the radiative properties of the clouds are not the determining factor in the appearance and disappearance of the ship tracks. While not appearing to play a role in the detection of the ship tracks, radiative properties seem to affect the strength of the cloud modification as shown by Platnick et al. (2000) and Taylor et al. (2000). Interestingly, the lack of influence by cloud radiative properties is consistent with inferences made earlier by Platnick and Twomey (1994), who noted that while many clouds were radiatively susceptible, they did not have ship tracks despite the ever present ship traffic. Here, however, even clouds that, based on their small cloud droplet effective radii, would seem to have low susceptibilities are nevertheless affected by the underlying ships.

To study further the possible links between radiative susceptibility and the appearance of ship tracks, the observations were searched for relationships between cloud cover, cloud droplet radii, optical depths, and the appearance of ship tracks. Figure 8 shows optical depths, cloud droplet radii, and cloud-top altitudes for pixels found to be overcast by low-level clouds within 60-km regions that contained ship track heads and those that did not. The observations are for the 60-km regions south of 35°N and east of 130°W. They are taken from the morning *NOAA-12* passes. As shown in Fig. 1, this region contained numerous ship tracks. Results for other regions and for the afternoon *NOAA-11* passes are similar. The results show that aside from the tracks appearing in the lowest of the low-level clouds, as noted earlier, the distributions of cloud droplet radii and optical depths are the same for clouds with and without ship tracks. Furthermore, no correlations between optical depth, cloud droplet radii, and cloud-top altitude are evident aside from a slight correlation between cloud droplet radii and cloud-top altitude for the clouds without ship tracks. This correlation, however, is peculiar to this region. It is absent for the regions either north of 35°N or west of 130°W. The correlation is thought to

arise from the lowest-level component of the low-level clouds being affected by continental air more so than the overlying upper-level component. In any case, the results shown in Fig. 8, and those for other regions (not shown), reinforce the finding that other than the difference in altitude, there appeared to be no difference between the clouds that exhibited tracks and those that did not.

The preference for ship tracks to occur in the southern portion of the domain, south of 35°N, can now be understood in terms of the cloud altitudes. Figure 9 shows the average surface pressure, surface temperature, and surface winds for June 1994 as derived from the 0000 UTC National Meteorological Center (NMC; now the National Centers for Environmental Prediction) analyses. The high pressure system and relatively cold waters of the eastern North Pacific are known to establish favorable conditions for the occurrence of stratus and stratocumulus (e.g., Klein et al. 1995). Figure 10 shows the standard deviation of the 0000 UTC surface pressure for June 1994. The standard deviation of the surface pressure field reflects the frequency with which weather fronts pass through the region, thereby disturbing the structure of the marine boundary layer. The standard deviation is high north of 35°N, where the occurrence of ship tracks is low. Figure 11 shows the average retrieved cloud-top altitude for the low-level clouds in June 1994, when they occurred as a single-layered cloud system that covered a substantial fraction (>10%) of a 2° × 2° latitude–longitude region. The cloud-top altitudes are higher where the standard deviations in surface pressure are higher. The higher average altitudes for low-level clouds are consistent with a boundary layer that is more frequently disturbed by the passage of low pressure systems (Stull 1988).

Why were more ship tracks observed in the *NOAA-12* satellite observations than in the *NOAA-11* observations? As is shown in Fig. 2, the tracks found in the *NOAA-12* imagery were more dense everywhere than the tracks found in the *NOAA-11* imagery. Figure 12 shows the relative frequencies for the fraction of pixels found to be overcast in 60-km regions that contained ship tracks (solid curve) and the fraction in the regions for which no ship tracks were observed (dashed curve). These regions fell between 30° and 45°N and between 140°W and the west coast of the United States. The observations were restricted to those with single-layered, low-level clouds that were everywhere below 1 km. The results shown in Fig. 12 indicate that the morning observations had a substantially higher fraction of overcast pixels than did the afternoon observations. The results in Fig. 12 also indicate that ship tracks were found more frequently when the number of overcast pixels was large (solid line). These results suggest that fewer tracks were found in the afternoon observations because of the breakup of the clouds. While it may be easier to identify ship tracks in overcast, rather than in broken, cloud systems, the fre-

NOAA−12

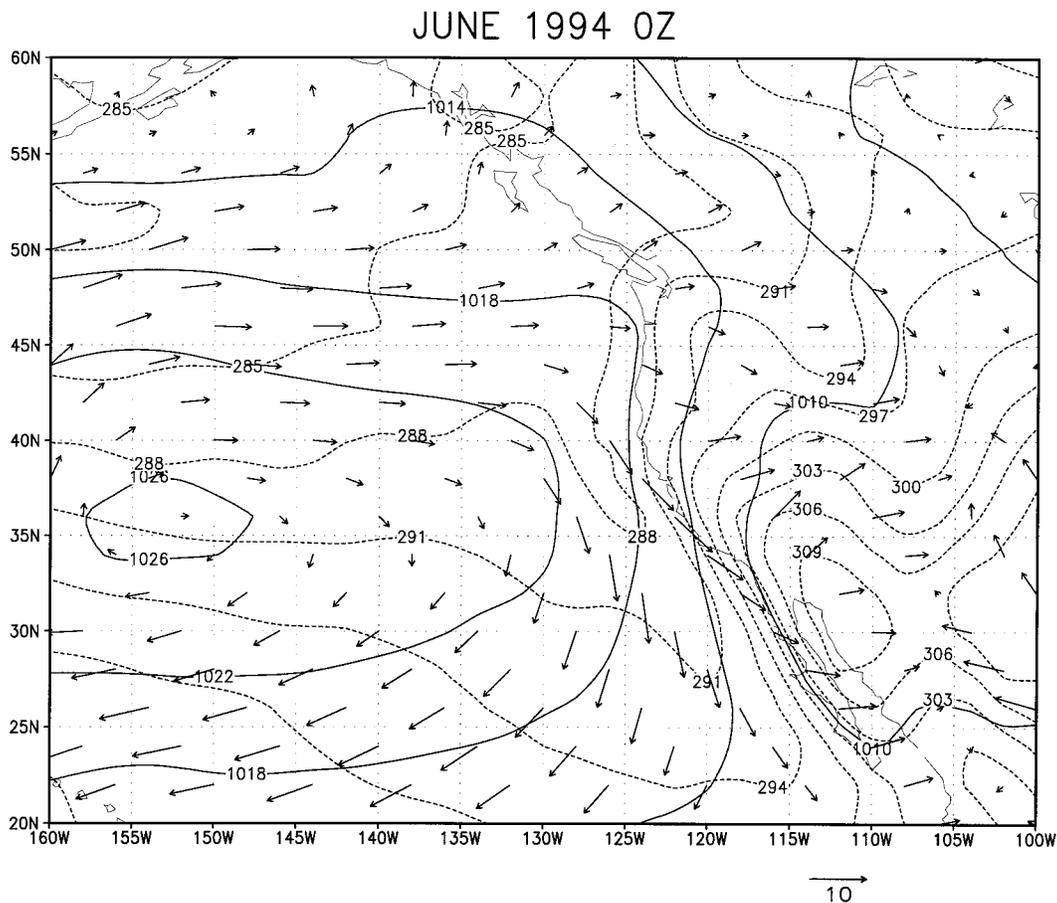SHIP TRACKS

NO SHIP TRACKS

JUNE 1994 0Z
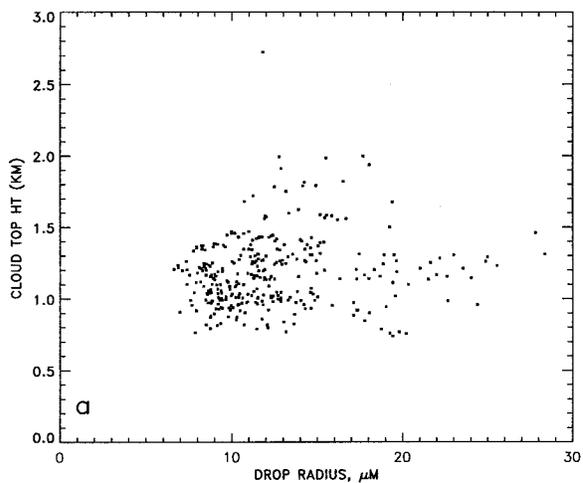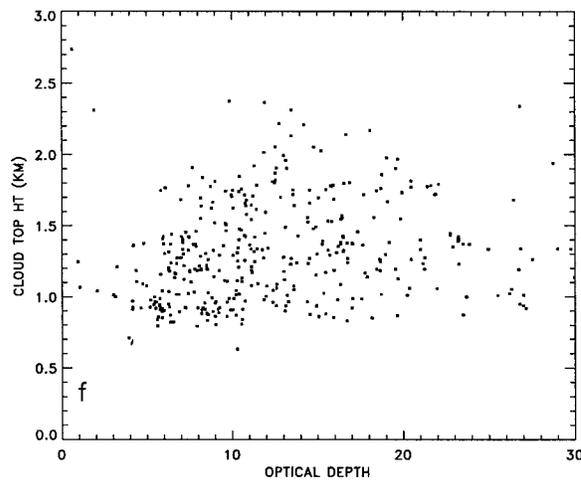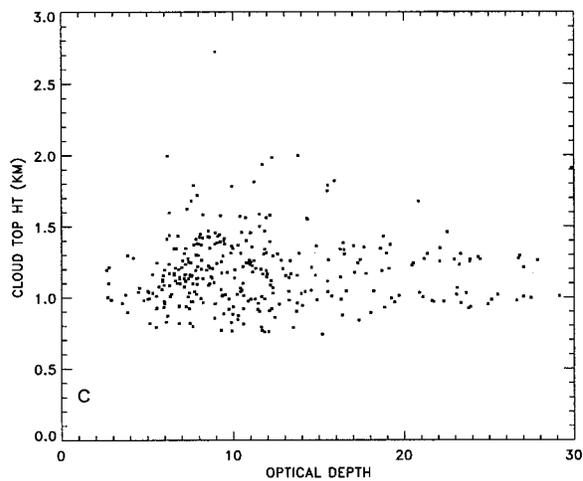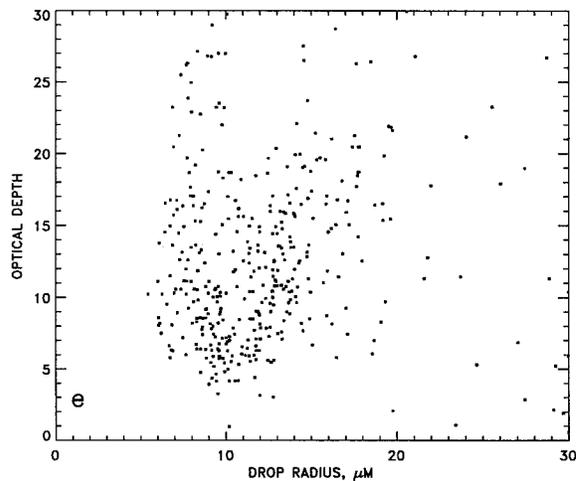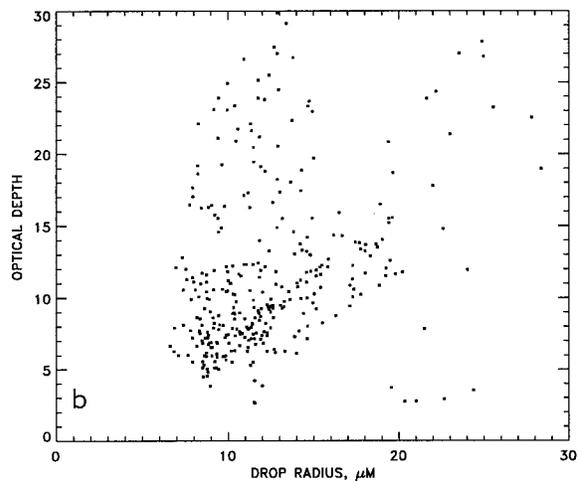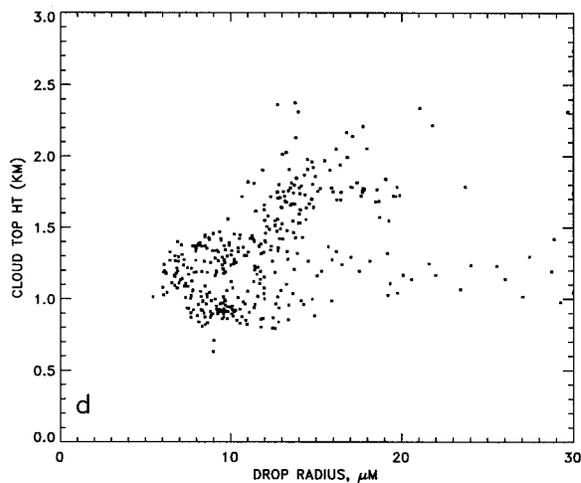
Fig. 9. Average surface pressure (mb), temperature (K), and winds (m s^{-1}) derived from 0 Z NMC analyses for Jun 1994.

quency of overcast pixels for clouds that are sufficiently low in altitude may also be indicative of the degree of coupling between the clouds and the underlying boundary layer. The studies of climatological records and the results of numerical simulations of the marine boundary layer noted earlier suggest that cloud cover is generally higher when the cloud layer is coupled to the boundary layer (Albrecht et al. 1995; Krueger et al. 1995a,b; Wyant et al. 1997).

The criterion that a large fraction of the pixels be overcast is, of course, not as well defined as the 1-km cutoff in cloud-top altitude. As indicated by the results in Fig. 12, many tracks can occur when clouds are mostly broken. Nevertheless, the probability of finding ship tracks is higher when low-level cloud cover is extensive and the frequency of overcast pixels is high. Also, as

with the altitude criterion, many pixels can be overcast by clouds that are sufficiently low and yet no tracks occur. Low altitude is evidently not a guarantee that the layer is coupled to the boundary layer.

The appearance of numerous ship tracks in the imagery of the *NOAA-11* afternoon pass on 14 June and the large drop in numbers on 15 June appears to be due to a marked shift in the altitudes of the clouds, as shown in Fig. 13. For the region between 25° and 35°N and east of 140°W, where most of the tracks were found, the clouds on 14 June were substantially lower in altitude than those on 15 June. Furthermore, the altitudes on 14 June were substantially lower than those typically observed for June 1994 in this region. The altitudes of the clouds on 15 June were more typical of the distribution of altitudes for the month. The fraction of over-

←

Fig. 8. The 0.63-μm optical depths, cloud droplet effective radii, and cloud-top altitudes derived for overcast pixels within 60-km regions and the fractional cloud cover of the regions for single-layered, low-level cloud systems that were within 50 km of a ship track head (a)–(c) and that were more than 200 km from a ship track head (d)–(f). The observations are for the morning *NOAA-12* overpasses of Jun 1994 over the region south of 35°N and east of 130°W. In order to facilitate comparison, the observations for the clouds without ship tracks were sampled so that the number of points shown is similar to the number shown for the clouds with ship tracks.

SURFACE PRESSURE STANDARD DEVIATION
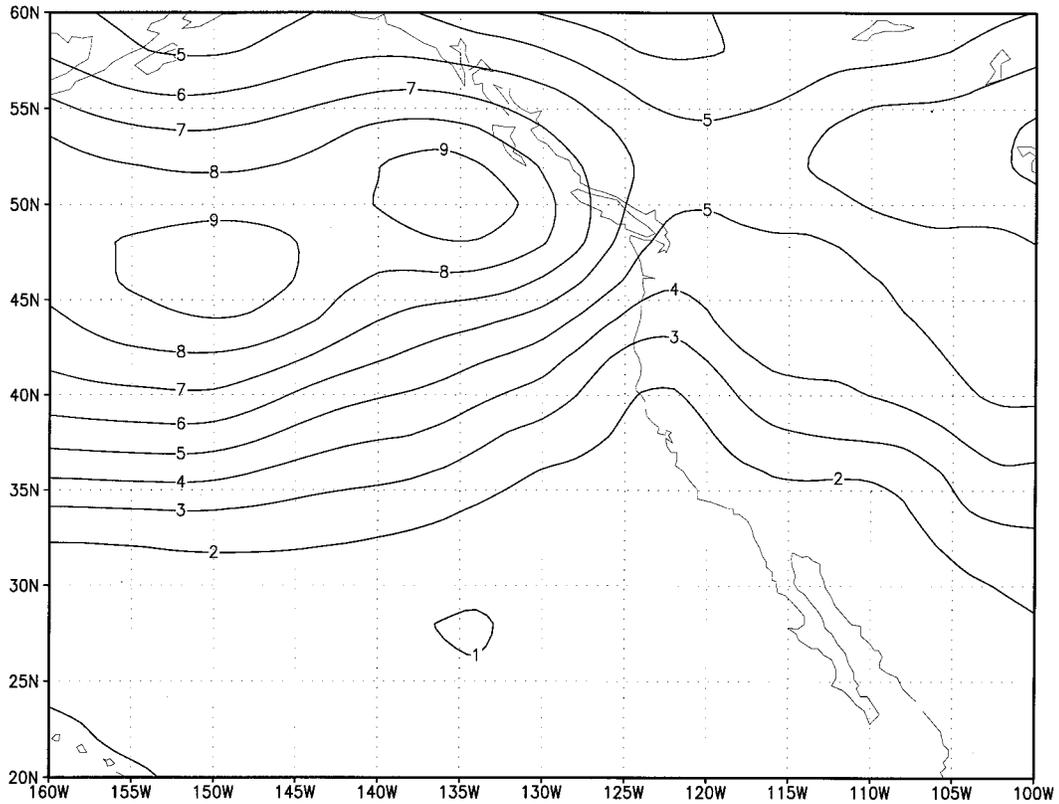### JUNE 1994 0Z

FIG. 10. Standard deviation of surface pressure (mb) derived from 0 Z NMC analyses for Jun 1994.
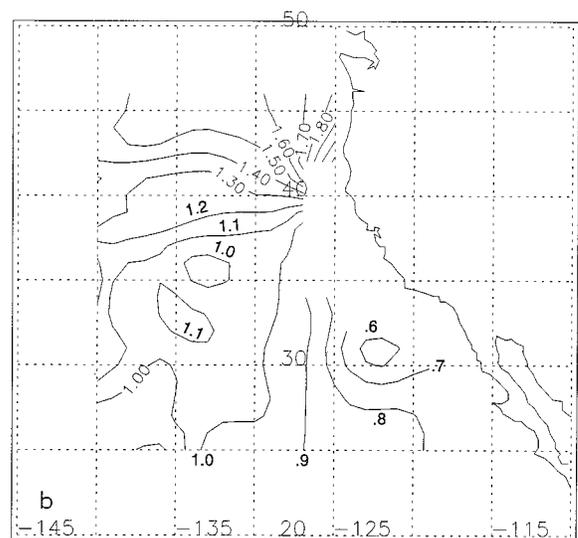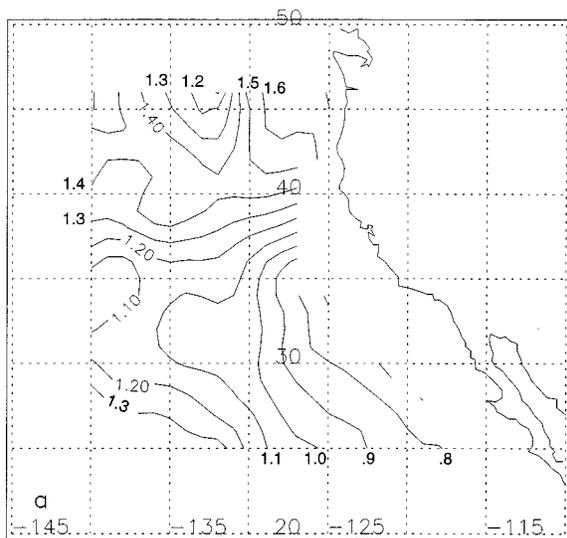
NOAA−12   NOAA−11

FIG. 11. Average retrieved cloud-top altitudes for 2° × 2° latitude–longitude regions that contained only low-level, single-layered cloud systems at the times of the satellite overpasses for the morning *NOAA-12* (a) and afternoon *NOAA-11* observations (b).
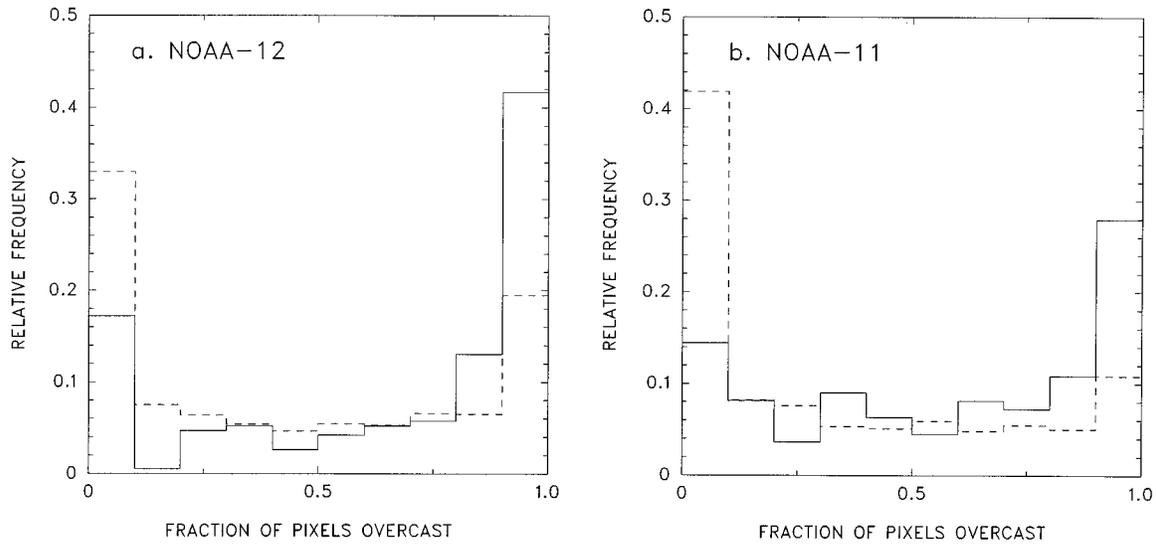
FIG. 12. Relative frequencies of overcast 1-km AVHRR pixels found within 60-km regions and for which the altitudes of the clouds were less than 1 km. Regions containing ship track heads (solid line); regions more than 200 km from a ship track head (dashed line). Morning *NOAA-12* observations (a) and afternoon *NOAA-11* observations (b). The observations are for ocean regions between 30° and 45°N and east of 140°W for Jun 1994.

cast pixels and the fraction of cloud cover were similar on both days.

5. Conclusions

The results presented here suggest that, at least for the west coast of the United States, whenever the altitude of the low-level clouds exceeds about 1 km, the occurrence of ship tracks in satellite imagery becomes exceedingly rare. The sensitivity of the occurrence of ship tracks to cloud altitude would appear to explain why ship tracks appeared predominantly in the southern portion of the region studied (south of 35°N). In addition, the results indicate that ship tracks are more prevalent when the low-level clouds are extensive so that a large fraction of the imagery pixels are completely cov-

ered by the clouds. A shift in cloud altitude appears to explain why many ship tracks were observed on 14 June, as shown in Fig. 3, when the low-level clouds were particularly low, but few on 15 June, even though the altitudes of the low-level clouds in the region where the ship tracks occurred were less than 1 km and the cloud cover and fraction of overcast pixels were similar on both days. While the distributions of cloud cover and cloud altitude were similar for the morning and afternoon observations, overcast pixels were more frequent in the morning observations; breaks in the clouds were more frequent in the afternoon observations. The higher frequency of overcast pixels for clouds sufficiently low for ship track formation to occur explains why more ship tracks were observed in the morning observations. If ship tracks disappear from satellite imagery when
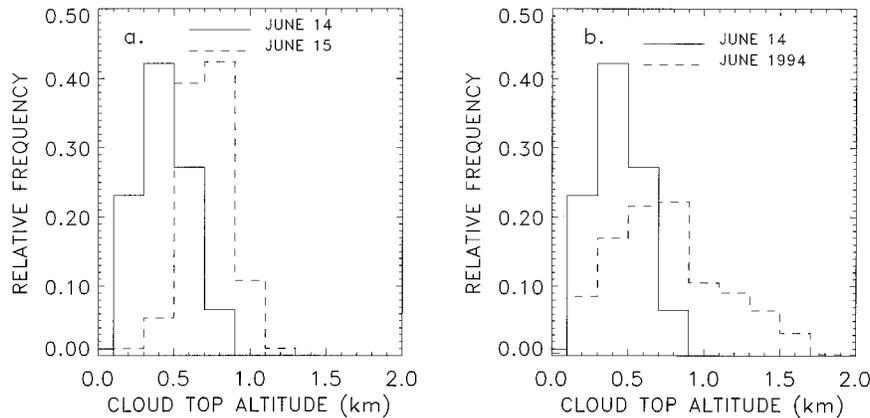

FIG. 13. Cloud-top altitudes for low-level clouds for the region between 25° and 35°N, and 140°W to the west coast, for 14 and 15 Jun (a), and for 14 Jun and the month of Jun 1994 (b).

low-level clouds become decoupled from or are poorly coupled to the boundary layer, as described by Nicholls (1984), then cloud altitudes as derived from satellite imagery and frequencies of overcast pixels for low-level clouds might serve as useful indices for distinguishing clouds that are coupled to the boundary layer from those that are decoupled or poorly coupled.

The effects of altitude and overcast pixels aside, the ranges of visible optical depths and cloud droplet effective radii for the clouds affected by ship tracks were similar to those that were unaffected. There appear to be no microphysical properties, as inferred from reflected sunlight at visible and near-infrared wavelengths, that would limit the appearance of ship tracks. All low-level clouds, whether they have large optical depths and small droplets or small optical depths and large droplets, appeared to be susceptible to the occurrence of ship tracks. The degree to which the clouds were modified, however, was not addressed here. Case studies of the degree of modification are dealt with by Taylor et al. (2000) and by Platnick et al. (2000).

REFERENCES

Albrecht, B. A., M. P. Jensen, and W. J. Syrett, 1995: Marine boundary layer structure and fractional cloud cover. *J. Geophys. Res.,* **100,** 14 209–14 222.

Arking, A., and J. D. Childs, 1985: The retrieval of cloud cover parameters from multispectral satellite images. *J. Climate Appl. Meteor.,* **24,** 322–333.

Betts, A. K., P. Minnis, W. Ridgway, and D. F. Young, 1992: Integration of satellite and surface data using a radiative–convective oceanic boundary-layer model. *J. Appl. Meteor.,* **31,** 340–350.

Coakley, J. A., Jr., and D. G. Baldwin, 1984: Towards the objective analysis of clouds from satellite imagery data. *J. Climate Appl. Meteor.,* **23,** 1066–1099.

Durkee, P. A., and Coauthors, 2000: Composite ship track characteristics. *J. Atmos. Sci.,* **57,** 2542–2553.

Fairall, C. W., A. B. White, J. B. Edson, and J. E. Hare, 1997: Integrated shipboard measurements of the marine boundary layer. *J. Atmos. Oceanic Technol.,* **14,** 338–359.

Han, Q., W. B. Rossow, and A. A. Lacis, 1994: Near-global survey of effective droplet radii in liquid water clouds using ISCCP data. *J. Climate,* **7,** 465–497.

Hobbs, P. V., and Coauthors, 2000: Emissions from ships with respect to their effects on clouds. *J. Atmos. Sci.,* **57,** 2570–2590.

Klein, S. A., D. L. Hartmann, and J. R. Norris, 1995: On the relationships among low-cloud structure, sea surface temperature, and atmospheric circulation in the summertime northeast Pacific. *J. Climate,* **8,** 1140–1155.

Kratz, D. P., 1995: The correlated *k*-distribution technique as applied to the AVHRR channels. *J. Quant. Spectrosc. Radiat. Transfer,* **53,** 501–517.

Krueger, S. K., G. T. McLean, and Q. Fu, 1995a: Numerical simulation of the stratus-to-cumulus transition in the subtropical marine boundary layer. Part I: Boundary-layer structure. *J. Atmos. Sci.,* **52,** 2839–2850.

——, ——, and ——, 1995b: Numerical simulation of the stratus-to-cumulus transition in the subtropical marine boundary layer. Part II: Boundary-layer circulation. *J. Atmos. Sci.,* **52,** 2851–2868.

Lauritsen, L., G. J. Nelson, and F. W. Porto, 1979: Data extraction and calibration of TIROS-N/NOAA radiometers. NOAA Tech. Memo. NESS-107, 73 pp. [Available from NOAA/NESDIS, Room 703, World Weather Building, Washington, DC 20233.]

Loeb, N. G., 1997: In-flight calibration of NOAA AVHRR visible and near-IR bands over Greenland and Antarctica. *Int. J. Remote Sens.,* **18,** 477–490.

McMillan, L. M., and D. S. Crosby, 1984: Theory and validation of the multiple window sea surface temperature technique. *J. Geophys. Res.,* **89,** 3655–3661.

Nakajima, T., M. D. King, J. D. Spinhirne, and L. F. Radke, 1991: Determination of the optical thickness and effective particle radius of clouds from reflected solar radiation measurements. Part II: Marine stratocumulus observations. *J. Atmos. Sci.,* **48,** 728–750.

Nakajima, T. Y., and T. Nakajima, 1995: Wide-area determination of cloud microphysical properties from NOAA AVHRR measurements for FIRE and ASTEX regions. *J. Atmos. Sci.,* **52,** 4043–4059.

Nicholls, S., 1984: The dynamics of stratocumulus: Aircraft observations and comparisons with a mixed layer model. *Quart. J. Roy. Meteor. Soc.,* **110,** 783–820.

Platnick, S., and S. Twomey, 1994: Determining the susceptibility of cloud albedo to changes in droplet concentration with the Advanced Very High Resolution Radiometer. *J. Appl. Meteor.,* **33,** 334–347.

——, and F. P. J. Valero, 1995: A validation of a satellite cloud retrieval during ASTEX. *J. Atmos. Sci.,* **52,** 2985–3001.

——, and Coauthors, 2000: The role of background cloud microphysics in the radiative formation of ship tracks. *J. Atmos. Sci.,* **57,** 2607–2624.

Prata, A. J., 1993: Land surface temperatures derived from the Advanced Very High Resolution Radiometer and the Along-Track Scanning Radiometer, 1. Theory. *J. Geophys. Res.,* **98,** 16 689–16 702.

Rao, C. R. N., and J. Chen, 1995: Inter-satellite calibration linkages for the visible and near-infrared channels of the Advanced Very High Resolution Radiometer on the NOAA-7, -9, and -11 spacecraft. *Int. J. Remote Sens.,* **16,** 1931–1942.

Stull, R. B., 1988: *An Introduction to Boundary Layer Meteorology.* Kluwer Academic, 666 pp.

Syrett, W. J., 1994: Low-level temperature and moisture structure from MAST: 5–29 June 1994. Pennsylvania State University Department of Meteorology Rep., 35 pp. [Available from Department of Meteorology, 503 Walker Building, The Pennsylvania State University, University Park, PA 16802.]

Taylor, J. P., M. D. Glew, J. A. Coakley Jr., W. R. Tahnk, S. Platnick, P. V. Hobbs, and R. J. Ferek, 2000: Effects of aerosols on the radiative properties of clouds. *J. Atmos. Sci.,* **57,** 2656–2670.

Weinreb, M. P., G. Hamilton, S. Brown, and R. J. Koczor, 1990: Nonlinearity corrections in calibration of Advanced Very High Resolution Radiometer infrared channels. *J. Geophys. Res.,* **95,** 7381–7388.

Wiscombe, W. J., 1977: The delta-M method: Rapid yet accurate radiative flux calculations for strongly asymmetric phase functions. *J. Atmos. Sci.,* **34,** 1408–1422.

Wyant, M. C., C. S. Bretherton, H. A. Rand, and D. E. Stevens, 1997: Numerical simulations and a conceptual model of the subtropical marine stratocumulus to trade cumulus transition. *J. Atmos. Sci.,* **54,** 168–192.